Effects of Wind on Convection in Strongly and Weakly Baroclinic Flows with Application to the Labrador Sea*

FIAMMETTA STRANEO, MITSUHIRO KAWASE,+ AND ROBERT S. PICKART

Department of Physical Oceanography, Woods Hole Oceanographic Institution, Woods Hole, Massachusetts

(Manuscript received 18 July 2001, in final form 25 February 2002)

ABSTRACT

Large buoyancy loss driving deep convection is often associated with a large wind stress that is typically omitted in simulations of convection. Here it is shown that this omission is not justified when overturning occurs in a horizontally inhomogeneous ocean. In strongly baroclinic flows, convective mixing is influenced both by the background horizontal density gradient and by the across-front advection of buoyancy due to wind. The former process—known as slantwise convection—results in deeper convection, while the effect of wind depends on the relative orientation of wind with respect to the baroclinic front. For the case of the Labrador Sea, wintertime winds act to destabilize the baroclinic Labrador Current causing a buoyancy removal roughly one-third as large as the air–sea buoyancy loss. Simulations using a nonhydrostatic numerical model, initialized and forced with observed fields from the Labrador Sea, show how the combination of wind and lateral gradients can result in significant convection within the current, in contrast with previous ideas. Though the advection of buoyancy due to wind in weakly baroclinic flows is negligible compared to the surface buoyancy removal typical of convective conditions, convective plumes are substantially deformed by wind. This deformation, and the associated across-front secondary circulation, are explained in terms of the vertical advection of wind-generated vorticity from the surface boundary layer to deeper depths. This mechanism generates vertical structure within the convective layer, contradicting the historical notion that properties become vertically homogenized during convection. For the interior Labrador Sea, this mechanism may be partly responsible for the vertical variability observed during convection, which modeling studies have until now failed to reproduce.

1. Introduction

Open-ocean deep convection occurs as a result of large surface buoyancy loss that is generally associated with large surface wind stress. For example, convection in the Labrador Sea and the northwest Mediterranean Sea is driven by wind outbreaks that advect cold, dry air off the continents at speeds often exceeding 20 m s^{-1} (Schott et al. 1996; P. Guest 2001, personal communication). So far, however, most simulations of deep convection have failed to include the effects of wind. This assumption is typically justified on the basis of scaling arguments since in the regime of deep convection the overturning is predominantly buoyancy driven and the mechanical stirring due to wind is comparatively unimportant. Neglect of the wind is also suggested by studies such as Harcourt et al. (2002), who studied convection in the interior Labrador Sea using Large Eddy Simulations (LES). In these simulations, however, as in many of the modeling studies of ''chimney convection,'' it is assumed that the convective region is void of any large-scale horizontal gradients. When this is not the case—given the relatively slow mixing timescales of deep convection (on the order of a day)—it is conceivable that wind will affect the mixing of properties. An understanding of the dynamical coupling of convective overturning, baroclinicity, and a surface wind stress is therefore necessary before these processes can be parameterized in models that are not capable of resolving small time and space scales.

The present study is motivated in part by two recent observations from the Labrador Sea, suggesting significant impact of wind and baroclinicity during convection. The first observation is that convection can occur within the boundary current on the western side of the Labrador Sea, previously believed to be a region where only limited overturning occurred because of the large vertical stratification there. The second observation is the high degree of vertical structure present during active convection in the interior of the Labrador Sea. This is contrary to the general assumption that convection results in complete vertical homogenization of proper-

* Woods Hole Oceanographic Institution Contribution Number 10609.

+ Current affiliation: Department of Physical Oceanography, University of Washington, Seattle, Washington.

Corresponding author address: Dr. Fiammetta Straneo, Dept. of Physical Oceanography MS. #21, WHOI, Woods Hole, MA 02543. E-mail: fstraneo@whoi.edu

ties. We argue how both of these features can be explained via the interaction of wind, baroclinicity, and surface buoyancy flux. This work is a natural extension of a previous study addressing the effect of the ocean's horizontal density gradients (baroclinicity) on convective mixing (Straneo et al. 2002, hereafter SKR) and of previous studies such as Haine and Marshall (1998). Straneo et al. demonstrated how convective plumes are deformed due to background horizontal gradients, which drives nonvertical mixing. Hence, parameterizations of convection as a one-dimensional mixing process in a baroclinic ocean can lead to erroneously shallow and light convective layers.

A recent hydrographic survey of the Labrador Sea during the winter convective season revealed that classical Labrador Sea Water (CLSW) can be formed within the western boundary current (Pickart et al. 2002, hereafter PCT). Specifically, deep mixed layers were observed in the offshore barotropic branch of the Labrador Current (Lazier and Wright 1993), in addition to the interior basin. Due to the difficult working conditions on the cruise, the inner baroclinic branch of the Labrador Current could not be properly sampled, hence it was impossible to determine the extent of overturning there. However, previous evidence suggests that convection can at times extend into the baroclinic branch of the Labrador Current as well. For example, an eddy of newly ventilated water, less dense than CLSW, was sampled in early spring near Flemish Cap (Pickart et al. 1996). This water mass, referred to as Upper LSW (ULSW), is believed to be the source of the middepth CFC maximum in the upper portion of the deep western boundary current. Pickart et al. (1997) argue that ULSW is formed by convective overturning in the baroclinic branch of the Labrador Current, which subsequently forms eddies due to baroclinic instability. Further evidence of convection in the baroclinic portion of the Labrador Current is provided by time series measurements from a succession of mooring deployments (see Rhines and Lazier 1995; Pickart et al. 1997).

The idea of convection in a baroclinic boundary current is somewhat new. Given the large vertical stratification, it has generally been assumed that convection, if any, would be very shallow. There is reason, however, to suggest otherwise. For example, SKR have shown that convection in a baroclinic flow deviates from one-dimensional mixing due to slantwise effects, which results in deeper mixed layers. Second, the strong winds that accompany convection will cause a lateral transport of buoyancy across a baroclinic current and, given the relatively slow timescales of convection, likely influence the deepening of the convective layer. For the case of the baroclinic Labrador Current, the prevailing northwesterly winds tend to advect dense water from offshore over lighter water, effectively destabilizing the water column. Convection in such a baroclinic boundary current is addressed in the first part of this paper. We examine the water masses formed in the inner branch of the Labrador Current and explore the relative contributions of slantwise and wind effects.

The second observation of interest from the Labrador Sea is the high degree of vertical structure observed within the convecting water in the interior of the basin. This was seen in both the hydrographic measurements (Pickart and Torres 1998) as well as in the Deep Lagrangian Float (DLF) data of Steffen and D'Asaro (2002). The hydrographic profiles revealed the presence of ''multiple mixed layers,'' whereby two (and sometimes three) uniform layers were vertically stacked upon each other (PCT). The profiles also contained a rich variety of intrusions interspersed throughout the mixed layers. Such variability (though generally less pronounced) was seen in the float data as well. A detailed comparison of the DLF measurements with ''model floats'' reveals that this vertical structure is one of the few features that LES simulations cannot reproduce (Harcourt et al. 2002). Convection in a weakly baroclinic interior ocean, in the presence of a surface wind stress, is addressed in the second part of the paper.

We employ a variety of data and models throughout the study. To address the problem of convection in a highly baroclinic flow we utilize the hydrographic measurements from the recent Labrador Sea Deep Convection Experiment (Lab Sea Group 1998). These data are used to determine the initial conditions and forcing fluxes appropriate for convection (section 2). This information is then used in a series of numerical runs addressing the convective layer deepening and water mass formation due to vertical mixing alone, slantwise convection, and wind (section 3). Finally, we investigate the combined effect of wind and baroclinicity on convection in the interior basin (section 4). The numerical model used is the same high-resolution, nonhydrostatic model employed by SKR, which assumes invariance along the direction of the mean flow.

2. The western Labrador Sea currents and forcing

a. Overview

The boundary current system of the Labrador Sea comprises a series of wind and buoyancy driven currents flowing cyclonically around the basin (Fig. 1). On the Labrador side, the baroclinic (inner) branch of the Labrador Current resides just offshore of the shelf break, centered above the 1000-m isobath. This buoyancy-driven current is supported by a hydrographic front separating cold, fresh arctic water from the warmer and more saline waters of subtropical origin. The width of the baroclinic Labrador Current is roughly 50 km and transports approximately 11 Sv (Sv $\equiv 10^6$ m^3 s^{-1}) (Lazier and Wright 1993). Seaward of this lies the barotropic (outer) branch of the Labrador Current located over the middle of the continental slope (Lazier and Wright 1993; Pickart et al. 1997). This is believed to carry the bulk of the subpolar Sverdrup return flow (order 26 Sv) in

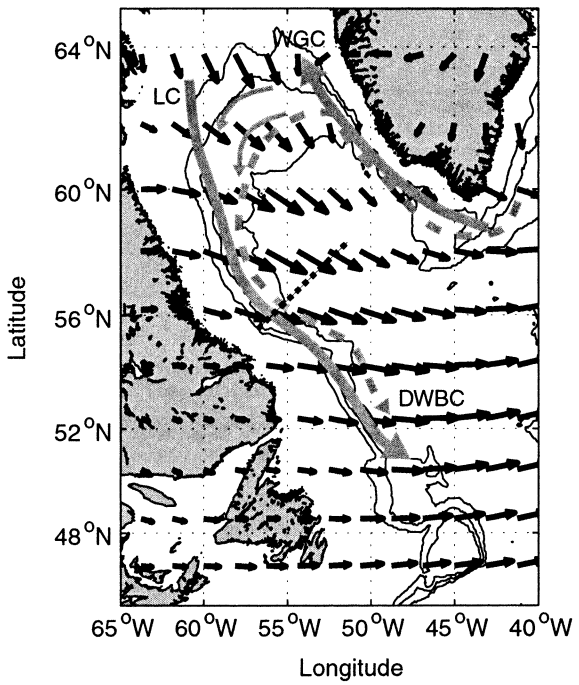

FIG. 1. Averaged 10-m winds for Feb–Mar 1997 from the NCEP reanalyzed dataset (courtesy of G. W. K. Moore). The dashed black line indicates the location of the repeat hydrographic section from the R/V *Knorr* wintertime cruise in 1997. Gray arrows indicate the approximate locations of the West Greenland Current (WGC; solid), the Labrador Current (LC; solid), and the bottom intensified DWBC (dashed). The bathymetric contours shown are 1000 m, 2000 m and 3000 m.

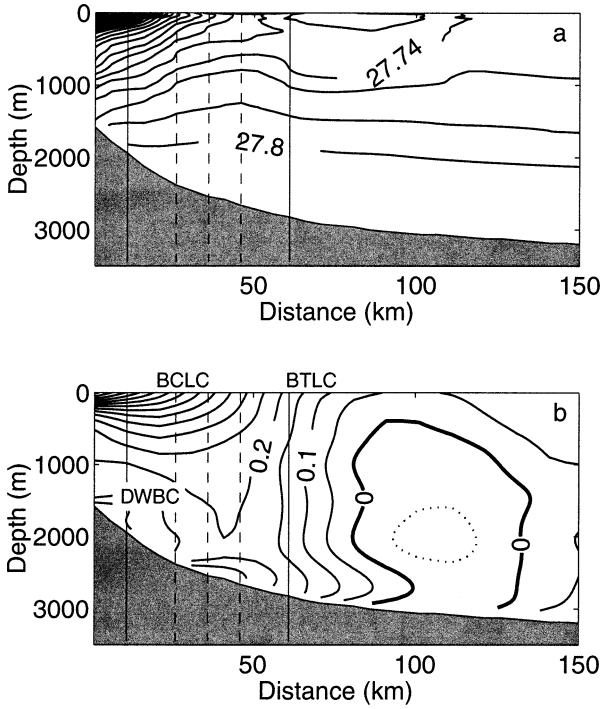

FIG. 2. Section II from the R/V *Knorr's* hydrographic survey taken on 25 Feb 1997. The location of the section is indicated in Fig. 1. (a) Potential density referenced to the surface (σ_0), contour interval is 0.02 kg m^{-3}. (b) Velocity perpendicular to the section, contour interval is 0.05 m s^{-1}, solid is equatorward, dashed is poleward. The locations of the baroclinic Labrador Current (BCLC), the barotropic Labrador Current (BTLC), and the deep western boundary current (DWBC) are indicated in (b). The portion of the section used to initialize the numerical simulations of section 3c is indicated by the vertical solid lines. The vertical dashed lines indicate the location of the three profiles shown in Fig. 5.

a very narrow jet (order 70 km). Throughout this study we refer to the baroclinic branch of the Labrador Current as the BCLC, and the barotropic branch as the BTLC. These should not be confused with the bottom-intensified deep western boundary current (DWBC), which is located farther downslope and transports overflow water from the Norwegian and Greenland Seas.

In wintertime the winds in the Labrador Sea are predominantly out of the northwest, resulting in cold, dry air being blown off the continent over the relatively warm ocean. This is exemplified by the average February–March wind field based on 20 years of National Centers for Environmental Prediction (NCEP) data[1] (Fig. 1). A similar mean field is shown in Fig. 5 of Lab Sea Group (1998) for the winter months (December–March) between 1968 and 1997. The winds in this quadrant are associated with the largest buoyancy losses in the subpolar North Atlantic, as shown by Lilly et al. (1999) in the analysis of European Centre for Medium-Range Weather Forecasts model results.

The recent wintertime hydrographic survey of the Labrador Sea was conducted during February and March 1997 aboard the R/V *Knorr* (PCT). As part of this survey, a section on the western side of the basin was occupied twice within a 10-day period [following (PCT), we refer to the first occupation as section II and the second as section IV]. The density and velocity distributions for section II are shown in Fig. 2. In this figure the BCLC is located roughly inshore of 40 km, and the BTLC between 40 and 80 km. The location of the section is shown in Fig. 1. A large buoyancy loss occurred between the first and second occupations, resulting in deepening convection in both the interior basin and in the BTLC. Because section IV did not extend into the BCLC, however, it was impossible to document the extent to which convection occurred in the BCLC. To make up for the lack of direct observations of convection within the BCLC, we use data from the first occupation as the initial density distribution, and model its evolution (in the next section) using surface fluxes derived as follows.

b. Buoyancy flux estimate

The surface buoyancy flux during the 10-day period between the two occupations can be estimated in a num-

[1] The NCEP heat flux fields have been calibrated using in situ measurements collected in the northwest Atlantic during winter 1996–97 (Renfrew et al. 2002).

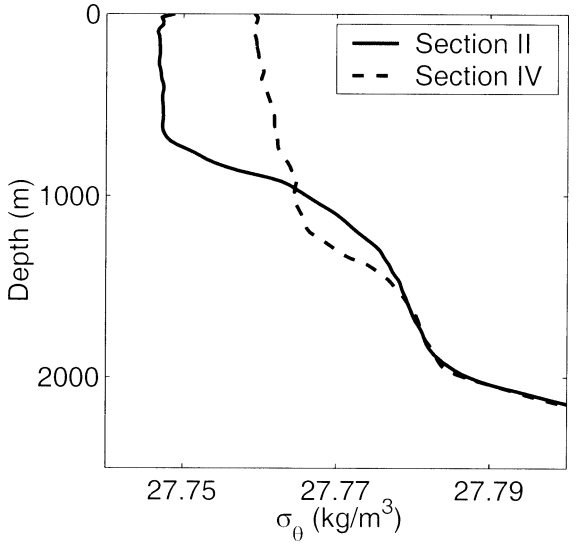

FIG. 3. Averaged σ_θ profiles for the Labrador Sea interior, from sections II and IV, taken on 25 Feb and 10 Mar 1997.

ber of ways. One could apply bulk formulae using directly observed meteorological and hydrographic variables. However, given the extreme wintertime weather conditions of the Labrador Sea these formulas are subject to considerable uncertainties (Renfrew et al. 2002). Instead, we use the difference in buoyancy content of the interior profiles between the two occupations to derive an approximate net buoyancy loss. This method relies on the assumption that lateral fluxes are negligible so that any difference is due to the surface flux alone. This is likely true only in the interior of the Labrador Basin where at least two of the processes driving lateral fluxes (slantwise convection and the advection of buoyancy by wind) can be neglected due to the small horizontal stratification. The net buoyancy loss is obtained by calculating the difference in the vertically integrated buoyancy content of the horizontally averaged interior profiles (those offshore of 100 km in Fig. 2) for the two sections (Fig. 3). By integrating from the surface to 2000 m we find this difference to be 9 kg m^{-2}.

If this change is assumed to be driven by a uniform surface buoyancy flux acting for 10 days, it yields an average flux of 10^{-7} m^2 s^{-3}. This is roughly equivalent to a heat loss of 490 W m^{-2} if the typical compressibility for the Labrador Sea is assumed to be 8.7×10^{-5} J kg^{-1} K^{-1} and under the assumption that the freshwater fluxes are negligible. The same calculation, repeated using the difference in the vertically integrated heat content (instead of total density), yields a similar mean heat flux of 450 W m^{-2}. Though we are implicitly neglecting the net buoyancy transport resulting from eddy activity, strong support for this value comes from measurements by Lagrangian floats that were released during the hydrographic cruise in roughly the same region (Steffen and D'Asaro 2002). The float measurements reveal that the mean heat flux during this time is within a range of 400–600 W m^{-2}.

c. Wintertime wind forcing

Realistic surface wind stresses can be obtained from direct atmospheric measurements collected during the hydrographic cruise (courtesy of P. Guest). Since the *Knorr* was away from the region of section II/IV between the two occupations, we do not have a direct measurement of the forcing in this area during the 10-day period. Instead, we use a representative wind stress obtained by averaging all the data from the cruise (approximately 40 days during the months of February and March) when the vessel was in the western half of the Labrador Sea. The mean wind stress calculated as such is 0.26 N m^{-2}, equivalent to a wind speed of 15 m s^{-1} from west-northwest. In terms of the effectiveness of the wind at transporting buoyancy across the BCLC, we are interested in the component of the wind that is parallel to the current. Taking this to be the direction of the isobaths, the magnitude of the mean wind stress along the axis of the BCLC is 0.17 N m^{-2} (equivalent to a surface wind speed of 12 m s^{-1}). Note that the wind direction computed for the winter of 1996/97 is more westerly than the 20-yr mean field of the Lab Sea Group (1998). Hence, the cross-frontal advection of buoyancy estimated below would be even greater for the case of a ''canonical'' winter in the Labrador Sea.

3. Convection in the boundary current system

We now use a series of models to address the extent to which convection can occur in the two branches of the Labrador Current, with particular focus on the BCLC. In all simulations the initial condition is provided by the first occupation of the hydrographic section (Fig. 2). Following the above analysis, we use a buoyancy flux of 10^{-7} m^2 s^{-3} and, unless otherwise stated, a surface wind stress of 0.17 N m^{-2}. In all cases we show results for two different forcing times, 10 and 20 days. The 10-day simulation represents the time that elapsed between the two hydrographic sections and hence provides us with a ''simulated completion'' of the repeated section (done on 10 March). We use the 20-day simulation as an estimate of the extent to which overturning may have occurred by the end of the convective season.

To investigate the contribution of different mechanisms in driving convection in the boundary current, we make use of a series of progressively more complex models. First we use a one-dimensional model to simulate overturning due to vertical mixing alone, which is driven solely by buoyancy flux. This scenario is in line with the results of Harcourt (1999) and others, who argue that the mechanical stirring due to wind is negligible in the interior of the Labrador Sea during convection. Next we investigate the impact on convection

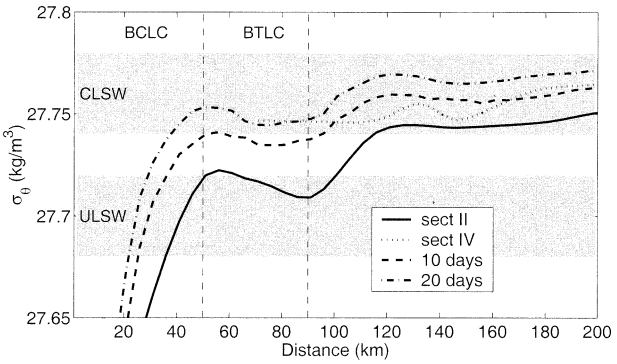

FIG. 4. Plot of σ_θ vs distance in the mixed layer for the one-dimensional model simulations after 10 and 20 days of forcing. Also shown is σ_θ at 100 m for sections II and IV, and the location of the baroclinic and the barotropic portions of the Labrador Current (BCLC and BTLC, respectively). Shaded regions indicate the density ranges for ULSW and CLSW.

due to the presence of horizontal stratification in the boundary current in conjunction with the wind stress. We use basic Ekman theory to argue that the wind-driven advection of buoyancy across the density front is nonnegligible. Finally we use a nonhydrostatic numerical model to investigate the deviation from vertical mixing due to slantwise convection and to the coupling of baroclinicity and wind effects.

a. One-dimensional mixing

In the first model we assume that a surface buoyancy loss results in the vertical homogenization of a layer of fluid (the mixed layer) and that there is no discontinuity at its base. The potential density distribution across the section, within the mixed layer, after 10 and 20 days of forcing is shown in Fig. 4. Included in the figure are the density ranges corresponding to ULSW (σ_θ = 27.68–27.72 kg m^{-3}) and CLSW (σ_θ = 27.74–27.78 kg m^{-3}), as defined by Pickart et al. (1997). The mixed layer model shows that CLSW can be formed in the BTLC, while water mass formation in the BCLC is limited mostly to ULSW—even in the 20-day forcing scenario. These results are in line with Pickart et al. (1997) who did a similar calculation using historical data. The mixed layer depths in the present simulation range from 100–700 m (150–900 m) in the BCLC to 800–900 m (1000 m) in the BTLC for 10 (20) days of forcing.

b. Impact of wind-driven lateral fluxes

The model presented above does not include the effects of the large wind stress that is parallel to the flow. Given the orientation of the BCLC and the surface stress, we expect the wind-driven advection of buoyancy to be directed onshore and hence to be effective at destabilizing the water column. How does this compare with the destabilization due to the buoyancy flux? For simplicity consider the case of an infinitely extended front characterized by a uniform horizontal density gradient σ_y, where y is the cross-stream coordinate. We assume that the surface stress acts over a layer of thickness d. Let Q be the surface buoyancy flux and τ the zonal component of the wind stress. According to laminar Ekman theory, the vertically integrated meridional transport V_E induced by the wind acting over the layer of thickness d is

$$V_E = -\frac{\tau}{f\rho_0}, \tag{1}$$

where f is the Coriolis parameter and ρ_0 is the reference density of seawater. To estimate the relative contribution of surface buoyancy flux versus wind, consider the rate of change of mass per unit area over the depth d. If we assume that the only lateral fluxes are those induced by wind, and given a surface buoyancy flux Q, this is given by

$$\frac{d}{dt}\int_{-d}^{0} \sigma\, dz = \frac{\rho_0}{g}Q + \sigma_y V_E = \frac{\rho_0}{g}Q - \sigma_y\frac{\tau}{\rho_0 f}. \tag{2}$$

The first term on the right-hand side of (2) accounts for the density change due to the surface buoyancy flux Q, which is positive for buoyancy leaving the ocean's surface, while the second term accounts for the buoyancy transport due to wind. In this term, the horizontal density gradient in (2) is a mean gradient, vertically averaged over the depth of the layer affected by the wind. For the BCLC, $\sigma_y > 0$ and $V_E < 0$ for a positive wind stress. Note, incidentally, that by the same argument we expect wind to have a stabilizing effect on the West Greenland Current. The ratio of the two terms for the BCLC can be calculated by using the parameters derived above ($Q = 10^{-7}$ m^2 s^{-3}, $\tau = 0.17$ N m^{-2}) and a mean horizontal density gradient of $\sigma_y = 2.5 \times 10^{-6}$ kg m^{-4}. This estimate of σ_y is obtained by vertically averaging the horizontal density gradient over the top 500 m at the center of the BCLC (the central profile in Fig. 2). This yields a ratio for the wind-driven buoyancy flux to the vertical buoyancy flux of

$$\frac{g\sigma_y\tau}{\rho_0^2 Q f} \approx 0.32. \tag{3}$$

Thus, based on this simple calculation, we expect the wind-induced lateral advection of buoyancy to provide an effective buoyancy loss that is approximately one-third that due to the surface flux. Note that this calculation does not include slantwise convection effects, nor does it account for any coupling of wind and baroclinicity that may modify the mixing. Yet this first attempt shows that, in regions of strong horizontal gradients, destabilization due to wind can make a substantial contribution to the net buoyancy loss.

c. Nonhydrostatic simulations

1) The numerical model

To study the effects of slantwise convection, and of the coupling of slantwise and wind effects on convection in the BCLC, we use a nonhydrostatic, high-resolution numerical model. It is the same model utilized by SKR to investigate slantwise convection in more idealized flows. Two important simplifications are made in formulating the model. First, it is assumed that subgrid-scale unresolved processes can be parameterized in the form of a constant Fickian diffusivity. This assumption, which has been employed in a number of convection studies (see SKR and references therein), can be justified on the basis that the model is capable of resolving the dominant mixing agents during deep convection—the convective plumes. Second, the model assumes invariance in one horizontal direction, making it more suited for problems where variations in one horizontal direction are much greater than in the other. This assumption is clearly satisfied in the boundary current regime, addressed in this part of the study. Regarding convection in the interior of the Labrador Sea, addressed in the second part of our study, the latter assumption is more applicable for larger gyrelike, baroclinic structures as opposed to smaller eddies. However, three-dimensional convective simulations that include wind show how convective cells tend to align along the wind direction, effectively becoming convective rolls (Harcourt 1999). This provides some support for the two-dimensional assumption made here.

As shown in SKR, the model is successful in producing plumes whose characteristics (width, velocities, and timescales) are in agreement with those observed at a number of deep convective sites. There are, nonetheless, a number of three-dimensional processes, such as baroclinic instability, or plume–plume interactions, which are not resolved in these simulations. While the model allows us to study the effect of wind on convective plumes in its simplest setting, we are not able to resolve how such processes couple with the dynamics described below—a question which needs further study. Regarding the role played by baroclinic instability during convection in the interior of the Labrador Sea, one should recognize that, while it likely impacts the spreading of convectively formed waters away from the formation region, previous studies of localized sinking may have unrealistically enhanced its effects (see Straneo and Kawase 1999). This notion is supported by the fact that recent wintertime observations from the Labrador Sea did not find a large number of convectively formed eddies, as one would expect from the classic chimney collapse scenario for the interior region (Lilly et al. 2002, submitted to *J. Phys. Oceanogr.*, hereafter LI).

Let x be the alongstream and y the across-stream directions then, by assuming no variations in the alongstream direction ($\partial/\partial x = 0$), the momentum equations can be written in terms u, the alongstream velocity, and ξ the zonal horizontal vorticity:

$$\frac{Du}{Dt} - f\upsilon = \nu_v\frac{\partial^2 u}{\partial z^2} + \nu_h\frac{\partial^2 u}{\partial y^2}$$

$$\frac{D\xi}{Dt} = f\frac{\partial u}{\partial z} + \frac{\partial b}{\partial y} + \nu_v\frac{\partial^2 \xi}{\partial z^2} + \nu_h\frac{\partial^2 \xi}{\partial y^2}, \quad (4)$$

where

$$\frac{D}{Dt} = \frac{\partial}{\partial t} + \upsilon\frac{\partial}{\partial y} + w\frac{\partial}{\partial z},$$

$$\upsilon = -\frac{\partial \psi}{\partial z}, \qquad w = \frac{\partial \psi}{\partial y}, \qquad \xi = \nabla^2\psi;$$

ν and κ are the eddy viscosity and diffusivity, and subscripts indicate horizontal and vertical coefficients. Note that the vorticity discussed throughout this section is that in the zonal direction, oriented perpendicular to the y–z plane, and should not be confused with the vertical vorticity that is more often referred to simply as vorticity in the oceanographic literature. Similarly, the streamfunction discussed below is in the vertical plane and should not be confused with the more familiar horizontal streamfunction. Finally, we assume a linear equation of state such that the conservation of buoyancy, $b = -g\rho'/\rho_0$, is given by

$$\frac{Db}{Dt} = \kappa_v\frac{\partial^2 b}{\partial z^2} + \kappa_h\frac{\partial^2 b}{\partial y^2}.$$

The model uses a staggered grid with the buoyancy and zonal velocity defined at the center of the grid rectangle, the meridional component of velocity at the sides, and the vorticity and streamfunction at the corners. The Prandtl number is one, and the horizontal and vertical eddy diffusivities are 5 $m^2\ s^{-1}$ and 0.03 $m^2\ s^{-1}$, respectively. The lateral grid spacing is 125 m, vertical grid-spacing 7 m, and the basin dimensions are 50 km by 2000 m. An Adams–Bashforth time stepping scheme is used with a 30-s time step. Boundary conditions are no flux for buoyancy for the lateral and bottom boundaries, while the flux condition at the surface is given by $Q(y, t) = -\kappa_v\partial b/\partial z$. Boundary conditions for the momentum equations are no stress at lateral boundaries, no slip at the bottom and $(\tau^x, \tau^y) = \rho_0\nu_z(u_z, \upsilon_z)$ at the surface. The wind stress $\boldsymbol{\tau}$ is given by

$$\boldsymbol{\tau} = (\tau^x, \tau^y) = c_D\rho_a|\mathbf{U}_w|\mathbf{U}_w,$$

where c_D is the drag coefficient (10^{-3}), ρ_a is the density of air (1.2 kg m^{-3}), and U_w is the wind velocity in m s^{-1}. In the simulations described below we take u to be the alongstream flow component and limit our attention to the effects of a surface stress that is parallel to the flow ($\tau^y = 0$). The surface stress, when present, is applied simultaneously along with the surface buoyancy flux. The model is initialized with the potential density and velocity fields from section II, limiting the domain to the onshoremost 50 km shown in Fig. 2, roughly

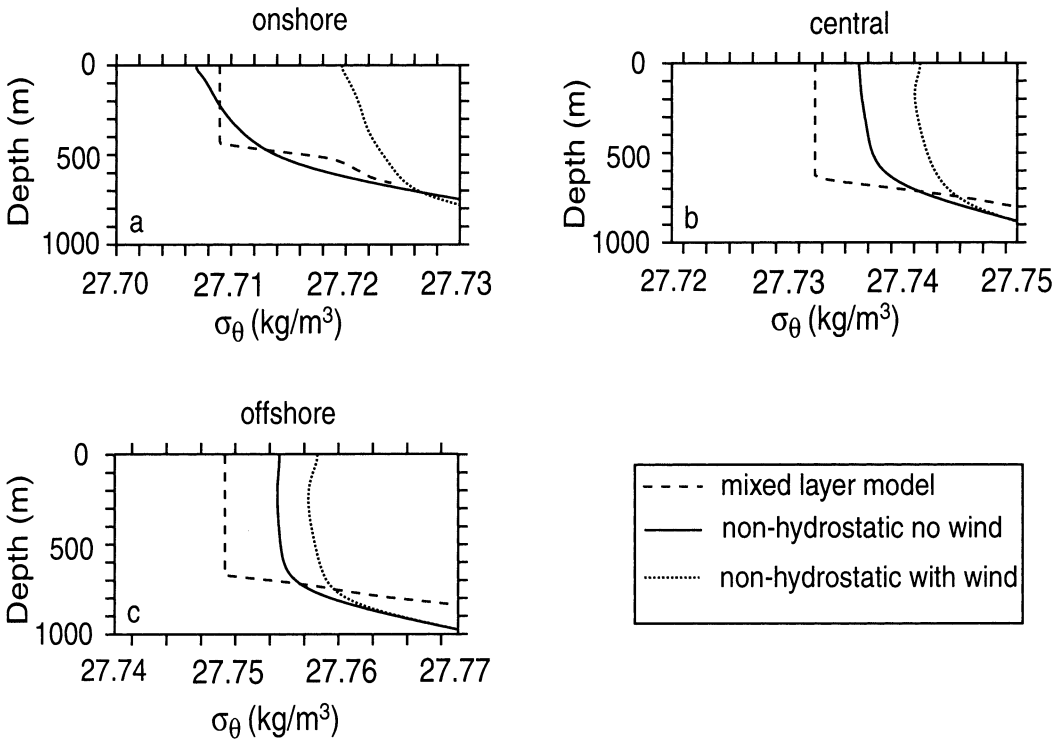

FIG. 5. Profiles of σ_θ after 20 days of buoyancy forcing for mixed layer model with no wind stress (dashed). nonhydrostatic numerical model with no wind (solid), and numerical model with wind (dotted). Locations for the three profiles shown, (a)–(c) are indicated in Fig. 2: (a) the onshoremost location and (c) the offshoremost.

coinciding with the BCLC. The surface forcing applied is 10^{-7} m^2 s^{-3} for the buoyancy flux and 0.17 N m^{-2} for the wind stress. A more detailed description of the model and its success at representing convective overturning can be found in SKR.

2) RESULTS

The numerical model provides us with a tool to investigate the convective layer modifications induced by slantwise effects as well as the coupling of baroclinicity and wind. This is done by comparing two different nonhydrostatic simulations: one in which the boundary current is subject to the buoyancy flux alone and one in which it is simultaneously subject to a buoyancy flux and a surface wind stress. In the buoyancy flux only simulation, we make the assumption that deviations from the mixed layer model dynamics discussed above are principally due to slantwise convection effects. In the buoyancy flux and wind forcing simulation, departures from the mixed layer model are due both to slantwise effects and to lateral advection of buoyancy by wind. Slantwise convection manifests itself in tilted plumes that drive mixing along the absolute momentum surfaces of the mean flow. Because the stratification along these surfaces is less than the vertical stratification, slantwise convection results in deeper mixing (compared to one-dimensional mixing) while maintaining a weak stable stratification (see SKR). According to SKR, these effects are significant only when the local gradient Richardson number, defined as the ratio of the vertical stratification to the square of the vertical shear in the alongstream velocity, is of order one (or equivalently when the stratification on the alongstream absolute momentum surfaces is different from the vertical stratification). Since both the horizontal and vertical stratifications vary across the front (Fig. 2), we expect the deviation in density and depth of the convective layer due to slantwise effects to vary as such. Similarly, we anticipate that the effect of wind will also vary across the front, for two reasons. First, the amount of buoyancy transported laterally is proportional to the magnitude of the horizontal buoyancy gradient [see (2)]. Second, the change in density within the convective layer is dependent on the thickness of the convective layer within which this denser fluid is mixed (greater impact on shallower mixed layers). Since both vertical and horizontal stratification in the BCLC are largest onshore, this is also the region where we expect to see the largest effect of wind. Given the orientation of the boundary with respect to wind, both slantwise effects and wind forcing will result in deeper and denser convective layers in the BCLC.

We begin the comparison by showing the density profiles, after 20 days of forcing, for the buoyancy flux only run, the wind plus buoyancy flux run, and the one-

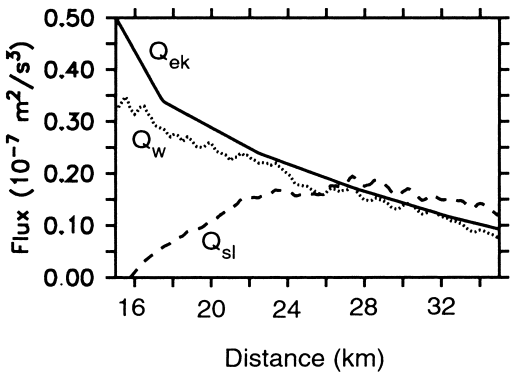

FIG. 6. Equivalent buoyancy fluxes due to slantwise effects (Q_{sl}, dashed) and wind effects (Q_w, dotted) from the nonhydrostatic simulations calculated after 20 days of forcing. The equivalent buoyancy flux from the Ekman model Q_{Ek} is the solid black line.

dimensional mixed layer model introduced in section 3a (Fig. 5). Profiles shown are taken at three different cross-stream locations, indicated in Fig. 2, and are representative of different regimes within the front. As the relative magnitude of the horizontal to the vertical stratification changes across the front, so too does the relative impact of wind and slantwise effects. At the most onshore location, wind causes the largest deviation in the mean density of the convective layer, while slantwise effects are unimportant. Hence the density profile in the buoyancy only run is identical to that of the mixed layer model (save for the slumping of the isopycnals), while in the wind and buoyancy forcing run the profile is on average 0.008 kg m^{-3} denser and clearly deeper (Fig. 5a). At the more central location, we see a departure from the mixed layer model even in the buoyancy only run (Fig. 5b), suggesting that slantwise effects are no longer negligible. When wind is included, the departure from the mixed layer is approximately doubled with respect to the buoyancy only run, suggesting that the effects of wind and of slantwise mixing on the convective layer are comparable. Finally, at the most offshore location, we see that slantwise convection still causes a noticeable departure from the mixed layer model, while wind effects are relatively less important (Fig. 5c).

To make a more quantitative comparison of the departure from vertical mixing due to slantwise effects and to wind, we modify (2) to include changes due to both processes. In practice, we ask what is the ''equivalent'' buoyancy flux, due to either process, in comparison to the surface buoyancy flux? To answer this question we assume that the two effects are essentially decoupled and that, when acting in combination, their effect can be represented as the superposition of their individual contributions. Let the rate of change of $S(x, t)$, the vertical integral of density (integrated over a depth greater than the convective layer), be

$$\frac{d}{dt}S(x, t) = \frac{d}{dt}\int_{-d}^{0} \sigma \, dz = \frac{\rho_0}{g}(Q + Q_{sl} + Q_w), \quad (5)$$

where Q is the atmospheric buoyancy flux, Q_{sl} is the equivalent buoyancy flux due to slantwise effects, and Q_w is the equivalent buoyancy flux due to wind. We now use the nonhydrostatic simulations to calculate both Q_{sl} and Q_w. Let $S_{mlm}(x, \bar{t})$, $S_{sl}(x, \bar{t})$, and $S_w(x, \bar{t})$ be the vertically integrated density at x, after 20 days of forcing, for the mixed layer model, the nonhydrostatic simulation with no wind, and that with wind, respectively. By integrating (5) in time, we can write expressions for the change in $S(x, t)$ in each of the runs.

$$\begin{aligned} S_{mlm}(x, \bar{t}) &= S_0(x) + \frac{\rho_0}{g}\int_0^{\bar{t}} Q \, dt = \frac{\rho_0}{g}Q\bar{t} \\ S_{sl}(x, \bar{t}) &= S_0(x) + \frac{\rho_0}{g}\int_0^{\bar{t}} (Q + Q_{sl}) \, dt \\ &= \frac{\rho_0}{g}(Q + \overline{Q}_{sl})\bar{t} \\ S_w(x, \bar{t}) &= S_0(x) + \frac{\rho_0}{g}\int_0^{\bar{t}} (Q + Q_{sl} + Q_w) \, dt \\ &= \frac{\rho_0}{g}(Q + \overline{Q}_{sl} + \overline{Q}_w)\bar{t}, \end{aligned} \quad (6)$$

where $S_0(x)$ is the initial vertical integral, and $\overline{Q}_{sl}$ and $\overline{Q}_w$ represent the time-averaged contribution of the slantwise and wind effects, respectively. The left-hand side of (6) is evaluated from the three runs and used to determine Q_{sl} and Q_w.

$$\overline{Q}_{sl}(x) = \frac{g}{\rho_0 \bar{t}}[S_{sl}(x, \bar{t}) - S_{mlm}(x, t)] \quad (7)$$

$$\overline{Q}_w(x) = \frac{g}{\rho_0 \bar{t}}[S_w(x, \bar{t}) - S_{sl}(x, \bar{t})]. \quad (8)$$

Finally, the equivalent buoyancy flux due to wind from the nonhydrostatic simulation, Q_w, is compared to that predicted by the laminar Ekman model, presented in section 3b [cf. (2)]:

$$\overline{Q}_{Ek} = \frac{1}{\bar{t}}\int_0^{\bar{t}} Q_{Ek} \, dt = -\frac{g}{\rho_0^2 f}\int_0^{\bar{t}} \tau\sigma_y \, dt.$$

Since the applied wind stress is constant in time, the horizontal density gradient is the only time varying quantity in the above expression. This term cannot be directly evaluated without an a priori knowledge of the convective layer's evolution, so we approximate it with the vertical average of the initial σ_y over the top 700 m of the water column (the convective layer due to wind varies between 600 and 800 m). A comparison of the three equivalent fluxes, after 20 days of forcing, is shown in Fig. 6. Only the interior portion of the domain is shown so as to eliminate the effects of the lateral

boundaries. Their magnitude should be compared to that of the applied surface flux, 10^{-7} m^2 s^{-3}.

This more quantitative analysis confirms the scenario described above. Slantwise effects are relatively unimportant onshore but increase to a maximum of 0.2×10^{-7} m^2 s^{-3} in the center of the front, thus amounting to a correction that is one-fifth of the magnitude of the atmospheric buoyancy flux (Fig. 6). This lateral variation in amplitude is due to the decreasing vertical and horizontal stratification across the front. At the most onshore location, slantwise effects are inhibited by the large vertical stratification; isopycnals are mostly horizontal on the plume scale, making mixing along the slanted paths formally identical to vertical mixing in terms of depth and density of the convective layer. Moving farther offshore, slantwise convection becomes more effective as the vertical stratification decreases but the horizontal stratification is still large. At the outer edge of the front the horizontal stratification decreases significantly; hence the impact of slantwise convection decreases accordingly. This behavior supports the analysis of SKR, who find that the importance of slantwise convection is determined by the relative magnitude of the horizontal to the vertical stratification. Wind effects—diagnosed from these numerical simulations—monotonically decrease in the offshore direction due to a reduction in the horizontal stratification (Fig. 6). The good agreement between Q_w and Q_{Ek} supports the assumption that the dominant effect of wind, in this boundary current regime, is due to the horizontal advection of buoyancy. The magnitude of the equivalent fluxes for slantwise and wind effects confirm that their impact is not negligible with respect to the surface buoyancy forcing. Indeed, their combined effect, over the central portion of the front, can amount to an equivalent increase in the buoyancy flux of approximately 50%.

We now return to our original question: how easy is it for convection to occur within the BCLC? Having shown that slantwise and wind effects can result in a substantial deviation from one-dimensional mixing, we illustrate how this affects the convective layer's depth and density distribution across the front. The depth of convection after 20 days of forcing in the three simulations is shown in Fig. 7. In the nonhydrostatic simulations, we use potential vorticity (PV) as an indicator of where convection has occurred; the low PV convected waters are separated from the unconvected waters by a large PV gradient. Slantwise effects result in a deeper convective layer than one-dimensional mixing. This departure is limited to a few tens of meters at the onshoremost part of the section, to about 100 m offshore. We note that the maximum in the convective layer depth in the one-dimensional model, located at the center of the section, is associated with horizontal inhomogeneities present in the original section data. This lateral structure is absent in the nonhydrostatic simulations because of the lateral mixing that has occurred during the 20 days of forcing. The impact of wind on the convective layer is much more pronounced. Wind stress results in a thickening of the convective layer by up to 300 m in the onshore portion of the BCLC, decreasing to zero offshore with respect to the slantwise only case (Fig. 7). This thicker convective layer is also associated with a denser convective product (Fig. 8). The combination of slantwise and wind effects results in a mean increase in the density of the water masses formed of approximately 0.01 kg m^{-3} (larger increases occurring onshore).

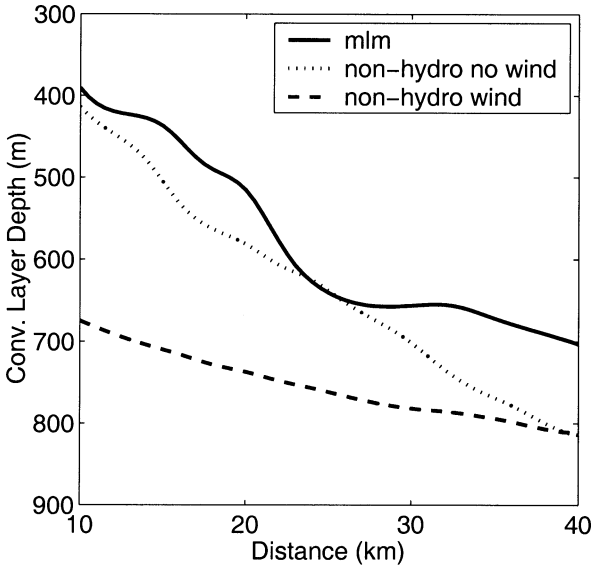

FIG. 7. Convective layer depth across the section after 20 days of forcing for the mixed layer model (mlm), the nonhydrostatic with no wind, and the nonhydrostatic with wind simulations. The portion of the section shown is that used to initialize the numerical simulations, shown in Fig. 2.

These simulations show that substantial convection in the boundary current is more likely than one might expect based on vertical mixing alone. This provides support to the theory that ULSW may be formed in the baroclinic branch of the Labrador Current (densities may even reach the CLSW range, Fig. 8). Our simulations are based on realistic wind and buoyancy forcing applied to observed hydrographic profiles from the wintertime Labrador Sea in 1997. It is worth noting that overall 1996/97 was a moderate winter (see PCT), hence such water mass formation is even more likely for robust winters, such as those which occurred earlier in the decade.

4. Convection in the interior

So far we have concentrated on the combined effects of baroclinicity and wind stress on convection in a strongly baroclinic flow. We have shown that the first-order effect of wind is a lateral advection of buoyancy that is significant with respect to the magnitude of the air–sea buoyancy flux. In this section, we examine the

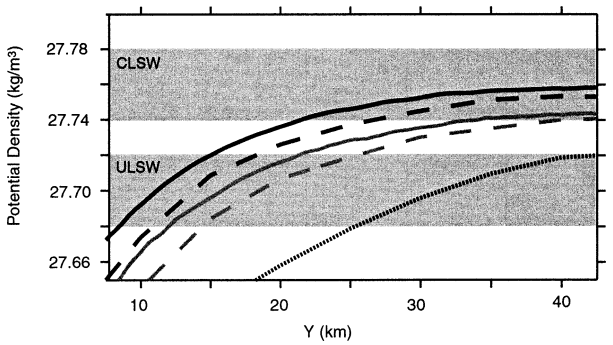

FIG. 8. Plot of σ_θ within the convective layer after 10 days (solid gray) and 20 days (solid black) of buoyancy and wind forcing from the numerical experiments. Mixed layer model density distributions (dashed lines) for the same forcing periods are the same as those shown in Fig. 4. The initial density distribution in section II (dotted line) was also shown in Fig. 4. Shaded areas represent the CLSW and ULSW density range.

impact of wind on convection in the interior of the Labrador Sea, where the bulk of CLSW is formed. Here, horizontal density gradients result from features such as eddies (LI) or horizontal recirculations (Lavender et al. 2000), with magnitude typically an order of magnitude less than that found in the baroclinic boundary current (PCT; LI). Because of this and because the surface buoyancy loss varies over larger spatial scales, we anticipate that the lateral advection of buoyancy due to wind is negligible with respect to the surface buoyancy flux. Instead, motivation for investigating the effect of wind on convection in the interior of the Labrador Sea is provided by the lack of an explanation for the large degree of spatial variability (especially vertical) observed during wintertime surveys of the interior Labrador Sea. Such variability was evident both in the towed CTD measurements undertaken in the winter of 1996/97 as well as in the measurements made by the convecting DLFs (Steffen and D'Asaro 2002). This variability is at odds with the notion that convection can be represented as a purely vertical mixing process. Even complex nonhydrostatic simulations of convection have, so far, been unable to reproduce it. For example, Harcourt et al. (2002) compared data collected by ''model floats,'' released in the LES simulations of convection in the Labrador Sea, with those collected by the DLFs (Steffen and D'Asaro 2002). Overall the agreement was excellent, except that the model floats were unable to reproduce the large degree of temperature variance observed by the DLFs while moving up and down the convective layer. As suggested by Harcourt et al., this, and other less dramatic discrepancies in the mean heat flux and vertical turbulent kinetic energy profiles found within the upper quarter of the mixed layer, may be due to the lack of large-scale temperature and salinity structures in the numerical simulations, and an omission of their interaction with wind stress.

One possible mechanism for the generation of the vertical temperature variance detected by both the hydrographic and the DLF measurements is slantwise mixing. As shown by SKR, the weak horizontal gradients observed in the interior are still large enough to drive mixing of properties along slanted paths, thus potentially creating vertical variability from horizontal structure. Straneo et al. did not, however, include the effects of a wind stress. In this section we extend the work of SKR to address how convective mixing in a weakly baroclinic flow (the interior Labrador Sea) is modified by a wind stress—in particular how the plumes are distorted. We use the same nonhydrostatic numerical model of the previous section and limit our attention to the case of a wind stress that is parallel or antiparallel to the mean flow since these conditions likely have the largest impact on the overturning. Because of the changing direction of the flow in a recirculation or an eddy, the orientation of the coordinate system is arbitrary. We therefore limit our attention to the case of a westward, surface intensified oceanic flow and address the case of a wind stress that is parallel or antiparallel to this flow. It should be recognized, however, that the results presented are only sensitive to the relative orientation of wind and of the oceanic flow, and not on their absolute direction.

a. Laminar Ekman layer in terms of vorticity

It is instructive to consider first the wind-only problem within the simplified framework of Ekman dynamics, which will then be compared to the full nonhydrostatic model. For our purposes, it is more appropriate to cast the laminar Ekman problem in terms of relative vorticity, as follows.

Let $\boldsymbol{\omega}$ be the relative vorticity vector,

$$\boldsymbol{\omega} = (\xi\, \eta, \zeta) = \nabla \times \mathbf{u} = (w_y - v_z, u_z - w_x, v_x - u_y),$$

where subscripts indicate partial derivatives. In terms of vorticity, the steady laminar Ekman balance, typically written as a momentum balance between the ageostrophic part of the Coriolis terms and the vertical viscous terms, becomes

$$f\xi = \nu_v \eta_{zz} \qquad f\eta = -\nu_v \xi_{zz}, \tag{9}$$

where we have neglected horizontal derivatives of the vertical velocity in comparison with vertical derivatives of the horizontal velocities. Boundary conditions for (9) are

$$\eta = \frac{\tau^x}{\rho_0 \nu_v}, \qquad \xi = -\frac{\tau^y}{\rho_0 \nu_v} \quad \text{at } z = 0 \quad \text{and}$$
$$\eta,\ \xi \to 0 \quad \text{as } z \to -\infty. \tag{10}$$

Solutions to (9), given (10) and assuming $\tau^y = 0$, are

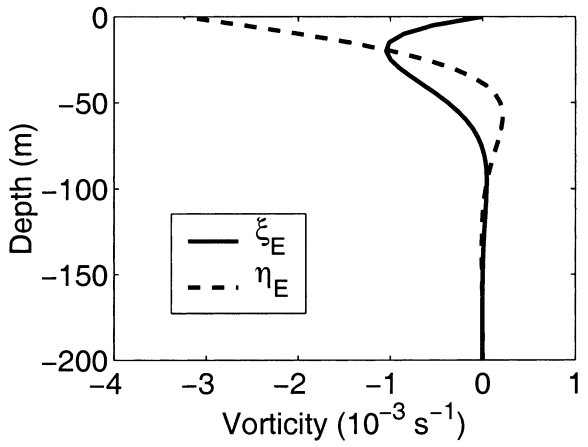

FIG. 9. Laminar Ekman solution in terms of vorticity [cf. (11)] for an easterly wind stress of 0.1 N m^{-2}.

$$\xi_E = -\frac{\tau^x}{\rho_0 \nu_v} e^{z/\delta} \sin\left(\frac{z}{\delta}\right) \quad \text{and}$$

$$\eta_E = \frac{\tau^x}{\rho_0 \nu_v} e^{z/\delta} \cos\left(\frac{z}{\delta}\right), \tag{11}$$

where $\delta = \sqrt{2\nu_v/f}$ is the Ekman layer depth.

Thus, in the vorticity framework, the laminar Ekman balance equates the tilting terms in the vorticity equation (representing the generation of one horizontal vorticity component due to the tilting of the planetary vorticity vector by the other) with the vertical viscous terms. Given this, (10) and (11) illustrate how an easterly wind stress is a source of meridional vorticity at the ocean's surface that, through the tilting of planetary vorticity vector, generates negative zonal vorticity within the Ekman layer. Fig. 9.

b. Nonhydrostatic model

Baroclinicity is the other factor that contributes to the evolution of zonal vorticity ξ, as seen in the last equation of (4). The term b_y represents the generation of vorticity due to a horizontal density gradient. The last two terms on the right-hand side of (4) represent the dilution of vorticity due to mixing. We now use the nonhydrostatic model to investigate the effects of baroclinicity and wind together.

We present results from four different experiments (see Fig. 10): an initially horizontally homogeneous ocean subject to a wind stress, nobcl; a weak baroclinic flow with no wind, nowind; the same baroclinic flow with a destabilizing wind, destab; and stabilizing wind, stab. The stabilizing (destabilizing) wind scenario refers to the case of an Ekman transport of buoyancy across the baroclinic front, which increases (decreases) the vertical stability. In all four experiments convection is driven by the same surface buoyancy loss of 2×10^{-7} m^2 s^{-3} applied for 3 days to an ocean whose vertical stratification is constant ($N = 3 \times 10^{-4}$ s^{-1}). For nowind, destab and stab, density decreases linearly to the north at a rate of 0.001 kg m^{-3}/km, and the flow is westward and surface intensified. These parameters are typical of wintertime conditions in the interior of the Labrador Sea, as discussed in SKR. Except where noted, a wind stress of 0.1 N m^{-2} is applied uniformly over the interior of the model domain, rapidly decaying to zero at the lateral boundaries. It is applied simultaneously with the surface buoyancy flux. Due to the lateral boundaries there is both a baroclinic and barotropic ''wind in a channel'' response. However, the barotropic flow does not affect the vertical structures, which are the focus here, and the baroclinic response is confined to a few kilometers of the lateral boundaries. To avoid such boundary effects, results are shown for the central portion of the domain only. It is important to recognize that in the interior the horizontal density gradients are typically an order of magnitude smaller than in the boundary current region. Hence the wind-transported buoyancy is negligible with respect to the surface buoyancy removal.

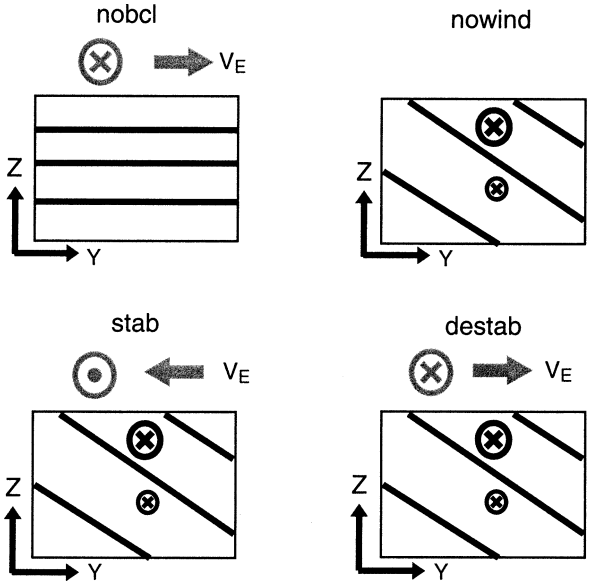

FIG. 10. Schematic representation of the four basic numerical experiments. Initial density distribution is in solid black and mean flow direction is shown as black circles. Wind stress is shown above vertical section in the gray circle, and the direction of Ekman transport V_E is indicated by the gray arrow.

1) VORTICITY BALANCE IN THE CONVECTIVE CELLS

In all the experiments a convective cell develops as a localized downward displacement of isopycnals within the surface thermal boundary layer. This localized displacement, associated with the sinking of dense fluid, generates vorticity of opposite sign on the two sides of

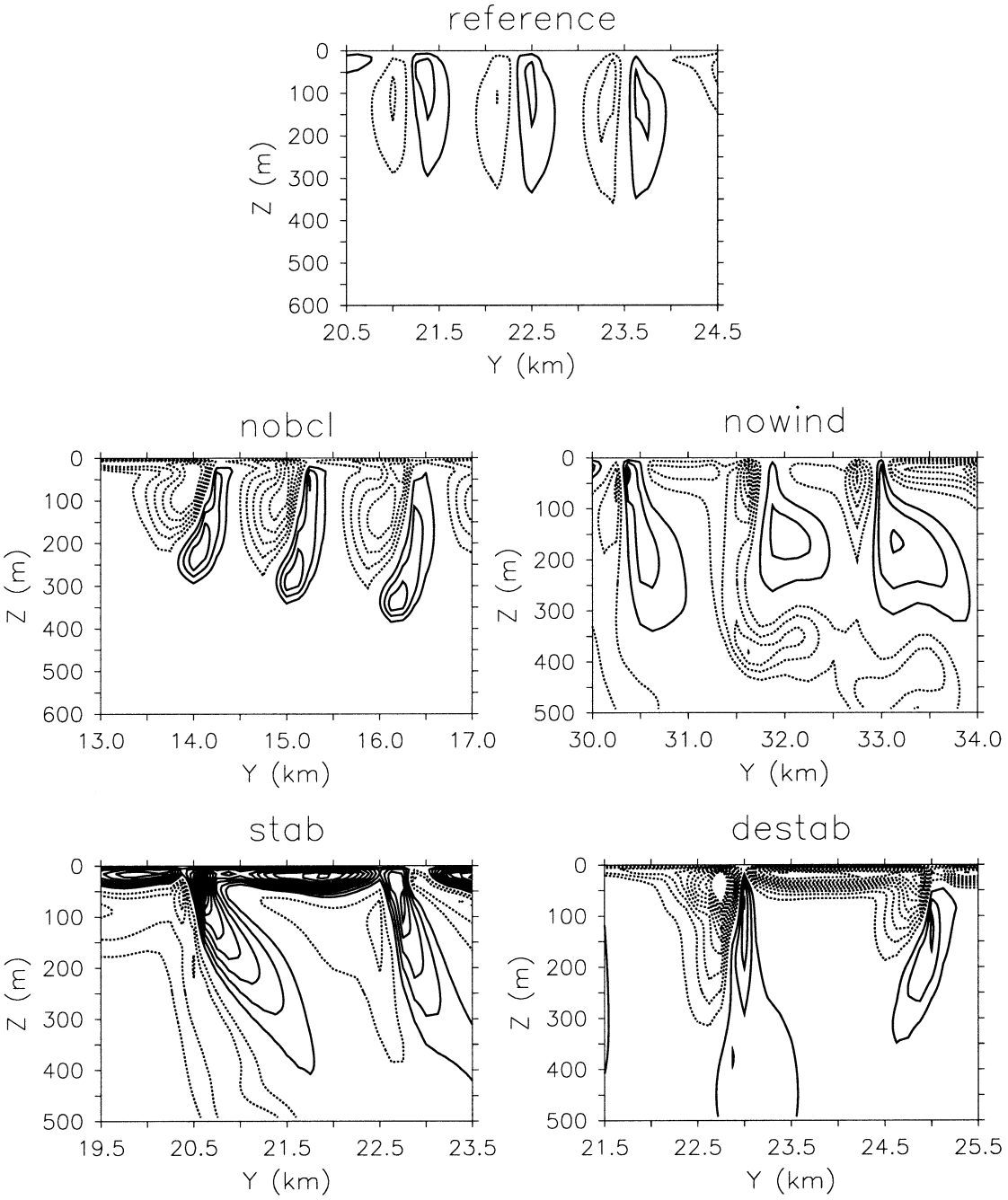

FIG. 11. Snapshots of the zonal relative vorticity for convective cells under different conditions (positive is solid. negative is dotted, contour interval is 2×10^{-4} s^{-1}). "Reference" indicates the experiment with no wind and no initial baroclinicity.

the dense core via the baroclinic term.[2] This vorticity is responsible for the broader and slower upwelling regions surrounding the sinking. Thus, in the absence of any background spatial inhomogeneities or wind stress, convective cells are symmetric about the vertical axis, and, in our zonally invariant scenario of rolls, are characterized by a positive and a negative vorticity lobe on either side of the sinking core. For the sake of comparison with the four experiments described above we show the typical signature of plumes in a scenario with no wind and no initial horizontal stratification (Fig. 11).

The addition of a wind stress implies, as argued above, the generation of a surface boundary layer of vorticity. For example, an easterly wind stress, as is

[2] The source of the baroclinicity in this case is the localized sinking of dense fluid, which is distinct from the baroclinicity resulting from a large-scale horizontal density gradient.

applied in nobcl, is a source of negative zonal vorticity in the Ekman layer (Fig. 9). Our experiments show how this surface layer of negative vorticity is continuously depleted as convective cells transfer vorticity from the boundary layer into the interior via vertical advection. This wind-generated vorticity advected out of the Ekman layer, in turn, causes the plumes to become vertically sheared (Fig. 11). Hence, of the two upwelling lobes surrounding the central sinking core, the one whose sign is the same as that generated by wind tends to dominate (Fig. 11). A parcel initially located at the surface will first be advected northward within the Ekman layer but, once entrained by sinking fluid and advected vertically out of the boundary layer, will move southward. While driving a similar vertical asymmetry in the plumes, this mechanism is essentially different from that of slantwise convection described in SKR. In the latter case the tilting of plumes occurs as a result of the baroclinic term due to the background horizontal stratification and the net effect is for fluid to sink and spread toward the lighter fluid (Fig. 11). When wind and background lateral stratification are both present, the two effects—baroclinicity and advection of surface vorticity—couple. In the stabilizing case these two vorticity producing terms are of the same sign resulting in strongly sheared plumes (Fig. 11). In the destabilizing case the two terms are of opposite sign, and the two mechanisms are in competition. In the latter scenario for typical interior Labrador Sea parameters, this amounts to quasi-vertical plumes (though not vertically uniform properties, see below).

It is important to realize that the magnitude of these two terms will, in general, vary with depth. For the background baroclinic term, the variation is dependent on any changes of the horizontal stratification with depth. In our experiments this term is set to be spatially uniform. The wind term, on the other hand, decays away from the surface as the vertically advected vorticity is diluted by mixing. Hence in our simulations, the vertical advection term tends to dominate in the upper portion of the convective layer, while the baroclinic term becomes more relevant in the lower portion. We can estimate the relative importance of the two terms by comparing their magnitude at the surface:

$$\frac{\text{wind}}{\text{baroclinicity}} = \frac{f\tau/\rho_0\nu_v}{B_y} \approx \frac{3 \times 10^{-7}}{10^{-8}} = 30,$$

where the magnitude of the wind term is estimated via the wind stress condition. Thus, close to the surface, the wind stress tends to dominate the vorticity evolution and is more effective in deforming plumes than a horizontal density gradient.

2) SECONDARY CIRCULATION

One of the effects of tilted plumes is the generation of a secondary circulation in the plane perpendicular to the direction of the mean current or mean wind. Vertical profiles of the meridional velocity, perpendicular both to the wind and to the baroclinic flow, are shown in Fig. 12 for the four scenarios. In each case the laminar Ekman solution for the meridional velocity[3] is shown as well. No secondary circulation develops in the no-wind and no-baroclinicity case (not shown). The model velocity profiles shown are obtained by averaging both in space, over the interior 30 km of the domain, and in time, over one day, during active convection. The averaging is necessary both to remove the plume variability and, more importantly, the inertial oscillations that are generated during convection. The amplitudes are reduced as a result of this averaging but retain their vertical structure.

Wind alone acting over an overturning ocean, nobcl, drives a laminar Ekman-type solution in the top layer and a weaker, broader return flow at depth within the convective layer (Fig. 12) due to the vertical advection of wind-generated vorticity. In the absence of wind, but in the presence of a horizontal stratification, nowind, the secondary circulation is the thermally direct one that is typical of slantwise convection (Fig. 12; see also SKR). Coupling of the baroclinic and wind effects generates a two-layer thermally direct circulation in stab (Fig. 12) and a three-layer circulation (thermally indirect above thermally direct) in destab (Fig. 12). In both cases the surfacemost flow is confined to the Ekman layer. The decreasing importance of wind effects away from the surface is evident in the direct circulation below the indirect one in the destabilizing case. A series of experiments with varying wind intensity reveal how the cross-over point between the thermally indirect and the thermally direct circulation becomes deeper with increasing wind speed (not shown).

It is conceivable that the secondary circulations shown above are capable of creating vertical structure in an ocean that previously had none or very little. To show this we introduced a passive tracer in the model, whose distribution can effectively show the cumulative effect of the secondary circulation. The tracer concentration is initially vertically homogeneous but linearly increasing toward the north. We plot profiles of tracer concentration anomaly that are averaged over the interior 30 km of the domain. In all of the runs with wind we show results for three different stress magnitudes: 0.05, 0.1, and 0.2 N m^{-2}. In the absence of a horizontal stratification the tracer anomaly distribution is solely due to tracer transport within the Ekman layer and subsequent vertical mixing of this anomaly within the convective layer. The net effect is a quasi-vertically homogeneous anomaly of tracer concentration within the mixed layer (Fig. 13). An increase or decrease in the wind stress simply enhances or decreases the anomaly. For the slantwise convection case, the thermally direct circulation results in a decrease (increase) in tracer con-

[3] This can be derived from (11) by assuming that the velocity tends to zero as $z \to -\infty$, and that $u_z = \tau/\rho_0\nu_v$ and $v_z = 0$ at the surface.

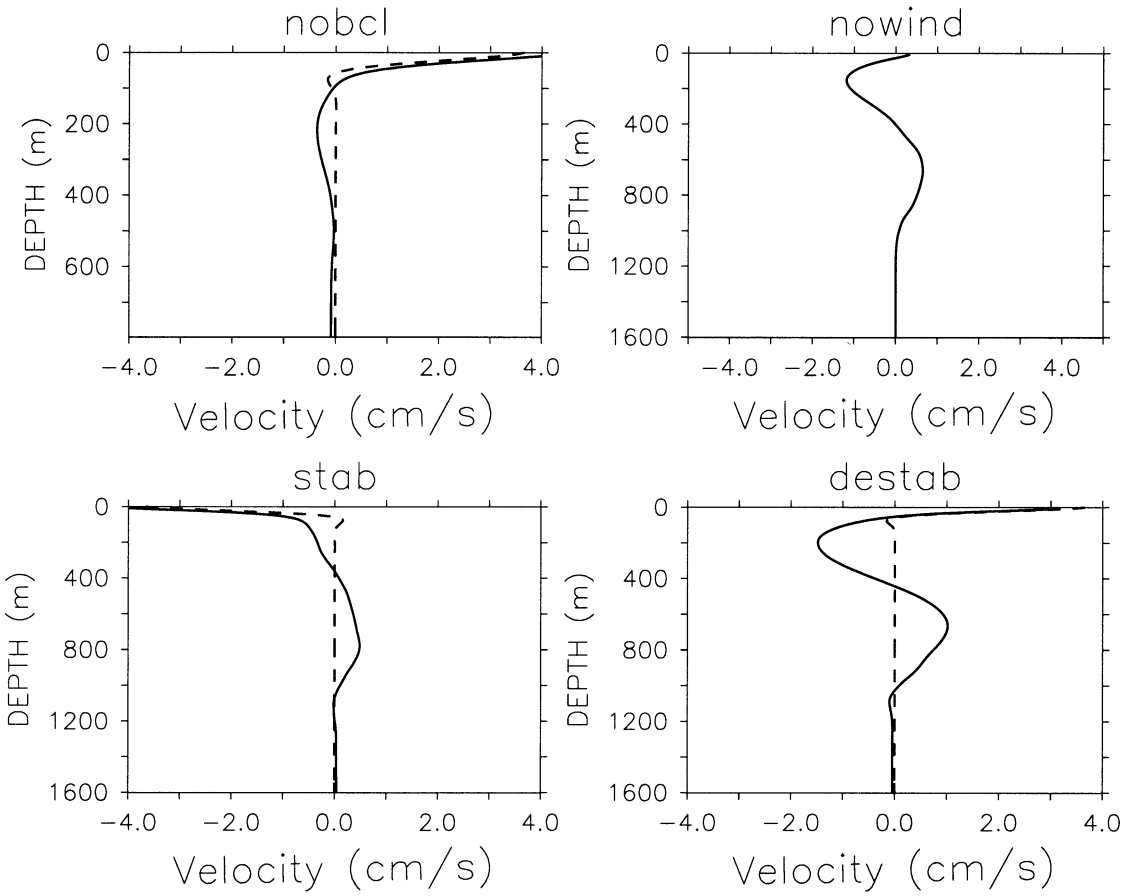

FIG. 12. Horizontally and temporally averaged profiles of the meridional velocity (solid) during convection for the four basic experiments. Overlaid is the laminar Ekman solution (dashed).

centration in the upper (lower) half of the convective layer (Fig. 13). This shows how vertical structure can be created via slantwise effects alone. The effect of wind can further enhance the creation of vertical structure through the strongly sheared cells in the stabilizing case (Fig. 13) or the more complex vertical structure of the flow in the destabilizing case (Fig. 13).

These simulations demonstrate that, under the action of baroclinicity and wind, convective plumes do not simply vertically homogenize quantities such as momentum or a passive tracer. This represents a dramatic departure from the often-used assumption that properties tend to be vertically uniform within mixed layers. Parameterization of these effects, then, cannot be easily achieved by simply increasing the magnitude of the vertical mixing over the depth of the convective layer. Instead, one might require a vertically varying eddy diffusivity, as well as one that evolves in time as the convective layer deepens. We were unable to diagnose such an effective eddy diffusivity using this model. This is in part due to the nonstationarity of the problem, given the continuously evolving convective layer, but also to the large degree of variability present in our simulations. Because of the limited domain, and of the inertial oscillations generated by the plumes, our model proved to be an inadequate tool for exploring how these effects could be parameterized. Finally, because of the two-dimensional assumption used in our simulations, it is impossible for us to predict how three dimensional processes, such as plume–plume interactions, may affect the vertical momentum and tracer concentration structures observed here. In general we expect the real ocean to be more turbulent than our relatively viscous model, and the effect of the smaller scales on the dynamics described here must be investigated with more sophisticated models. If, however, wind effects tend to deform plumes into roll-like structures, as observed in the LES simulations of Harcourt (1999), the two-dimensional results presented here should indeed apply.

5. Conclusions

This study has addressed the role of wind in convection in strongly and weakly baroclinic flows, a problem that finds a natural application in the Labrador Sea boundary current system and interior. In the first part of the paper we showed, using simple Ekman dynamics, that the advection of buoyancy due to wind can be

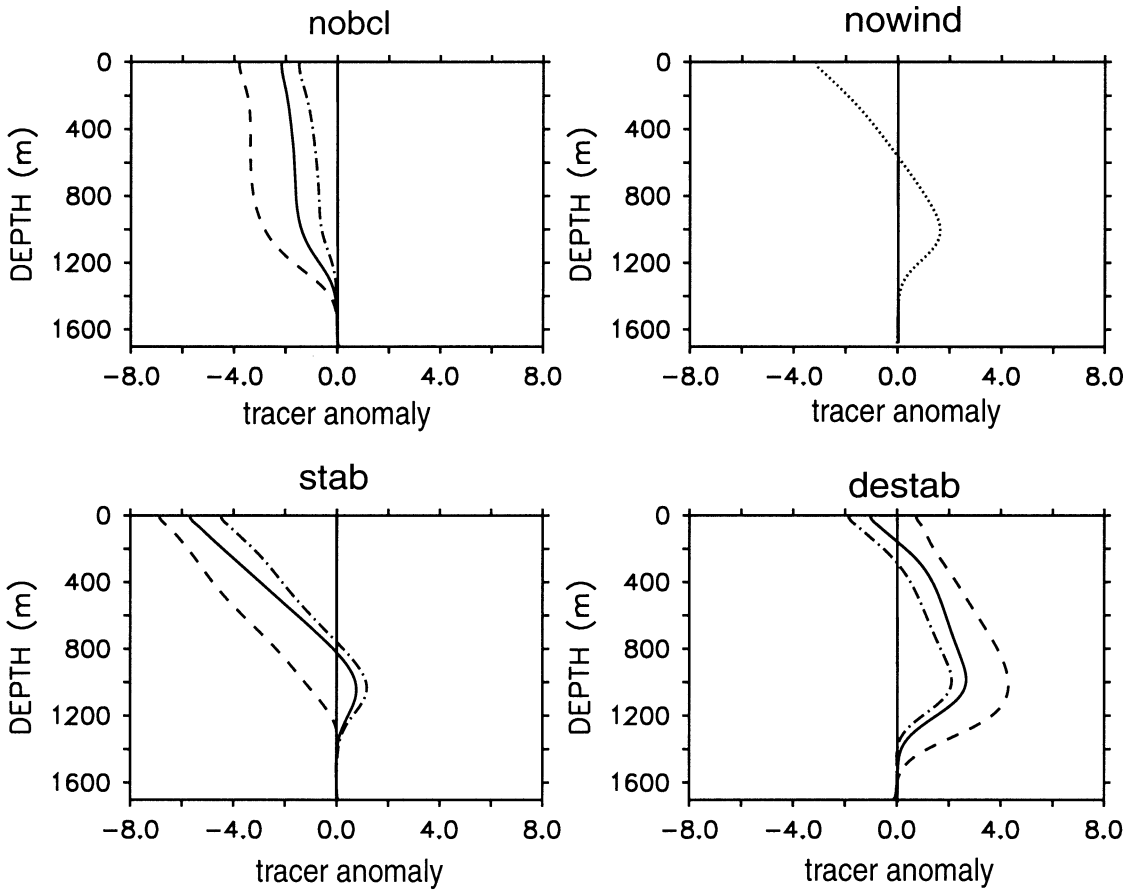

FIG. 13. Vertical profiles of tracer concentration anomaly (horizontally averaged) for the four basic experiments. When wind is applied, results from three different magnitudes of wind stress are shown: τ (in N m^{-2}) = 0.1 (solid), 0.2 (dashed), 0.05 (dash–dot). The zero line is shown for reference.

roughly one-third the size of the surface buoyancy flux in the strongly stratified baroclinic Labrador Current. Therefore, wind effects should not be neglected when considering convection in such a flow. Furthermore, in agreement with the slantwise convection scenario of SKR, we find that the baroclinicity of the Labrador Current results in a deeper and denser convective layer compared to the one-dimensional mixing prediction. The combined effects of wind and baroclinicity suggest that intermediate convection can occur within the baroclinic portion of the Labrador Current, resulting in densities within the upper LSW range, which may even reach the classic LSW range. While the specifics of our analysis are pertinent to the baroclinic Labrador Current, the mechanisms discussed here can be generalized to any baroclinic boundary current subject to large surface buoyancy flux and wind stress. In light of the results of Spall and Pickart (2001), who argue that the net sinking of dense fluid within the meridional overturning circulation mostly occurs at boundaries, we speculate that wind-facilitated convection in boundary currents may be a sizable fraction of the total dense water mass flux.

In the second part of the paper we addressed the dynamics of convective mixing in the presence of weak baroclinicity and wind—applicable to the interior Labrador Sea. This process leads to asymmetric development and deformation of the convective plumes. The plumes remove wind-generated vorticity from the surface Ekman layer and advect it to deeper depths, which explains both the resulting plume distortion and the secondary circulation that develops. This in turn gives rise to a pattern of mixing within the convective layer that generates vertical structure, as was demonstrated using a passive tracer. The resulting vertical gradients contradict the classic idea of convection as a means of vertically homogenizing the ocean, which is in line with recent observations from the Labrador Sea.

This study has shown, for two different oceanic regimes, that convective mixing cannot be decoupled from the larger scales. It has also highlighted the shortcomings of simple one-dimensional mixing schemes in a baroclinic flow field. This suggests that parameterizations of convective processes need to be verified against nonhydrostatic experiments in scenarios that are different from the idealized horizontally homogeneous scenarios within which they were developed. Because of

the simplifications made, we are not able to address how the dynamics described here can modify, or be modified by, three-dimensional processes such as vortex–vortex interaction and by baroclinic instability. This needs to be addressed with more complex models.

Acknowledgments. FS would like to thank the School of Oceanography of the University of Washington, Seattle, and R. W. Sternberg, in particular, for support while completing a portion of this work. RP was funded under Contract N00014-97-1-0043 from the Office of Naval Research.

REFERENCES

Haine, T. W. N., and J. Marshall, 1998: Gravitational, symmetric, and baroclinic instability of the ocean mixed layer. *J. Phys. Oceanogr.,* **28,** 634–658.

Harcourt, R. R., 1999: Numerical simulation of deep convection and the response of drifters in the Labrador Sea. Ph.D. thesis, University of California, Santa Cruz, 367 pp.

——, E. Steffen, R. W. Garwood Jr., and E. A. D'Asaro, 2002: Fully Lagrangian floats in Labrador Sea Deep Convection: Comparison of numerical and experimental results. *J. Phys. Oceanogr.,* **32,** 493–510.

Lab Sea Group, 1998: The Labrador Sea Deep Convection Experiment. *Bull. Amer. Meteor. Soc.,* **79,** 2033–2058.

Lazier, J. R. N., and D. G. Wright, 1993: Annual velocity variations in the Labrador Current. *J. Phys. Oceanogr.,* **23,** 659–678.

Lavender, K., R. E. Davis, and W. B. Owens, 2000: Mid-depth recirculation observed in the interior Labrador and Irminger Seas by direct velocity measurements. *Nature,* **407,** 66–69.

Lilly, J. M., P. B. Rhines, M. Visbeck, R. Davis, J. R. N. Lazier, F. Schott, and D. Farmer, 1999: Observing deep convection in the Labrador Sea during winter 1994–95. *J. Phys. Oceanogr.,* **29,** 2065–2098.

Pickart, R. S., and D. J. Torres, 1998: Wintertime hydrography of the Labrador Sea during active convection. *Eos, Trans. Amer. Geophys. Union,* **79,** OS174.

——, W. M. Smethie Jr., J. R. N. Lazier, E. P. Jones, and W. J. Jenkins, 1996: Eddies of newly formed upper Labrador Sea Water. *J. Geophys. Res.,* **101** (C9), 20 711–20 726.

——, M. A. Spall, and J. R. Lazier, 1997: Mid-depth ventilation in the western boundary current system of the sub-polar gyre. *Deep-Sea Res.,* **44,** 1025–1054.

——, R. A. Clarke, and D. Torres, 2002: Hydrography of the Labrador Sea during active convection. *J. Phys. Oceanogr.,* **32,** 428–457.

Renfrew, I., G. W. K. Moore, P. S. Guest, and K. Bumke, 2002: A comparison of surface-layer and surface turbulent-flux observations over the Labrador Sea with ECMWF analyses and NCEP reanalyses. *J. Phys. Oceanogr.,* **32,** 383–400.

Rhines, P. B., and J. R. N. Lazier, 1995: A 13-year record of convection and climate change in the deep Labrador Sea. *Atlantic Climate Change Program: Proceedings of the PI's Meeting,* A. M. Wilburn, Ed., University Corporation for Atmospheric Research, 57–64.

Schott, F., M. Visbeck, U. Send, J. Fischer, L. Stramma, and Y. Desaubies, 1996: Observations of deep convection in the Gulf of Lions, northern Mediterranean, during the winter of 1991/92. *J. Phys. Oceanogr.,* **26,** 505–524.

Spall, M. A., and R. S. Pickart, 2001: Where does dense water sink? A subpolar gyre example. *J. Phys. Oceanogr.,* **31,** 810–826.

Steffen, E., and E. D'Asaro, 2002: Deep convection in the Labrador Sea as observed by Lagrangian Floats. *J. Phys. Oceanogr.,* **32,** 475–492.

Straneo, F., and M. Kawase, 1999: Comparisons of localized convection due to localized forcing and to preconditioning. *J. Phys. Oceanogr.,* **29,** 55–68.

——, ——, and S. Riser, 2002: Idealized models of slantwise convection in a baroclinic flow. *J. Phys. Oceanogr.,* **32,** 558–572.